Electronic Supplementary Material (ESI) for Chemical Communications.

Supporting Information

In-situ potential-regulated architecture of ultrafine Ru-based electrocatalyst for ultralow overpotential lithium-oxygen batteries

Liangyu Jin,[a] Aiming Xing,[a] Zhenjiang Zhu,[a] Kui Fu,[a] Meng Zhou,[a] Fancheng Meng,[a] Xiangfeng Wei,[b] and Jiehua Liu*[ac]

a. Future Energy Laboratory, School of Materials Science and Engineering, Hefei University of Technology, Hefei 230009, China. E-mail: liujh@hfut.edu.cn, liujh@iccas.ac.cn

b. School of Chemistry and Chemical Engineering, Hefei University of Technology, Hefei 230009, China.

c. MOE Engineering Research Center of High-Performance Copper Alloy Materials and Processing, Key Laboratory of Advanced Functional Materials and Devices of Anhui Province, Hefei 230009, China.

1. Preparation of ultrafine Ru-based cathode

The Co-NC material was synthesized using the previously described process.[S1] The active material (Co-NC), conductive agent (Super P), and 5 % graphene ink were mixed with a weight ratio of 8:1:1 to form a slurry ink. Co-NC cathode was prepared by coating the slurry on commercial carbon paper (TGP-H-060) and drying it at 60 ℃ for 24 h. Anhydrous $RuCl_3$ electrolyte was obtained when $RuCl_3$ was dissolved in 1 M LiTFSi/TEGDME electrolyte in an argon-filled glovebox. Li-ion cell was assembled with Co-NC cathode, Li slice, and $RuCl_3$ electrolyte. Ultrafine Ru-based cathode was synthesized when direct galvanostatic discharging to 1.5 V by Neware battery tester. The Ru/Co-NC-H cathode was obtained with the same conditions, except with Co-NC washed in acid to remove Co on the surface of Co-NC, with details as follows. Co-NC powders were treated in 1 M HCl solution for 12 hours at 60 ℃. The final product (Co-NC-H) was then collected, washed with water/ethanol, and then dried at 60 ℃ for 24 h.

2. Materials characterizations

The morphologies and microstructures of as-prepared samples were characterized by SEM (SU 8020), FESEM (Gemini 500), and TEM (JEM-2100F with a HAADF-STEM detector and an Oxford EDS). The crystal structure was analyzed by XRD (PANalytical X-Pert PRO MPD) equipped with Cu Kα radiation (λ = 1.54056 Å). The surface elemental composition and chemical state was characterized by XPS (ESCALAB250Xi) analysis. The surface areas of the samples were measured using the Brunauer-Emmett-Teller (BET, Autosorb-IQ3) method based on N_2 adsorption-desorption employed with a micromeritics apparatus.

3. Assembly and electrochemical testing of LOBs

Different from lithium batteries, LOBs use CR2032 coin cells with order small holes (diameter: 1 mm) on the cathode side to facilitate oxygen diffusion. LOBs were assembled with a lithium slice, a piece of glass fiber separator (Whatman GF/D), the as-prepared ultrafine Ru-based cathode, and 1 M $LiClO_4$/DMSO electrolyte (160 μL) without any additives in an argon-filled glovebox. The galvanostatic electrochemical test was carried out on the Neware battery tester. CV curves were conducted on an electrochemical workstation (DH 7006, Donghua test) at a scan rate of 0.1 mV s^{-1} within a voltage range from 2.2~4.5 V. EIS measurements were performed at a frequency range of 1.0×10^5 Hz to 0.1 Hz with an amplitude voltage of 5 mV. The mass loading of Ru on the cathode is about 0.20 mg, and the specific capacity and current density are calculated on this basis. In addition, LOBs with the Co-NC cathode were assembled for comparison. The assembled LOBs were placed in a self-made container filled with pure O_2 for 6 h before electrochemical testing.

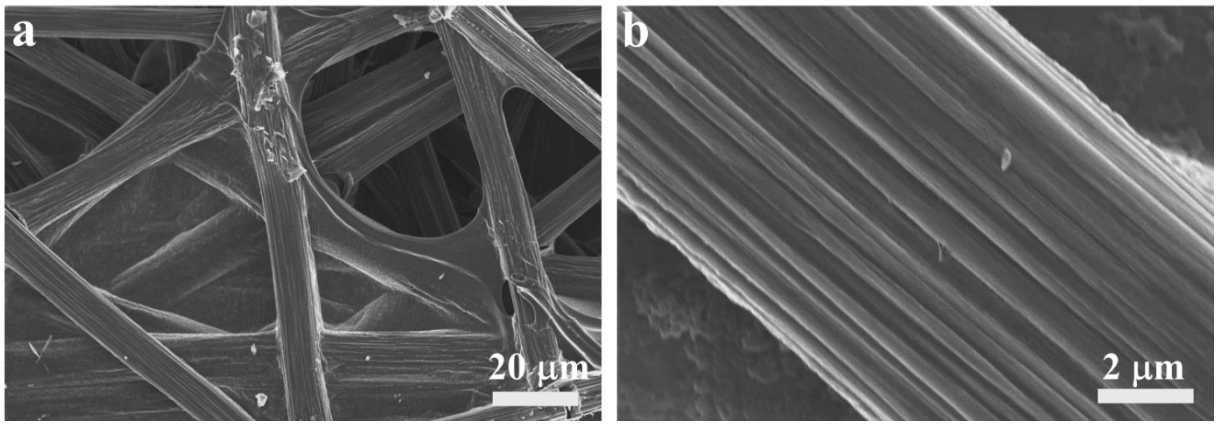

Fig. S1 (a-b) SEM images of CP at different magnifications.

Field emission scanning electron microscopy (FESEM) images of carbon paper (CP) have a network structure composed of carbon fibers with a diameter of about 5–10 μm in **Fig.** S1.

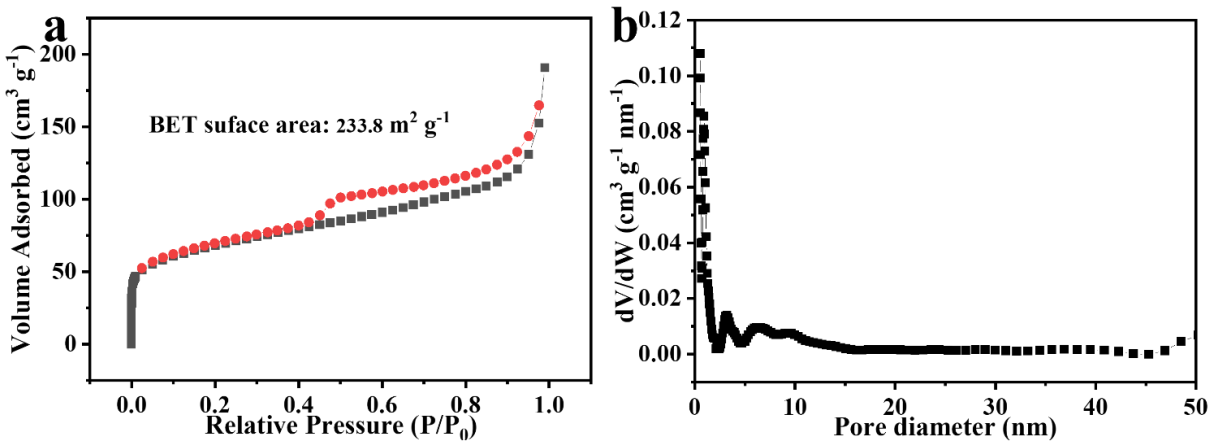

Fig. S2 (a) N_2 adsorption-desorption isotherms and (b) the pore size distribution of Co-NC.

The Co-NC material has also a hierarchical micro-mesoporous structure (**Fig.** S2), which is much higher than Super P (58.6 m^2 g^{-1}).[S2]

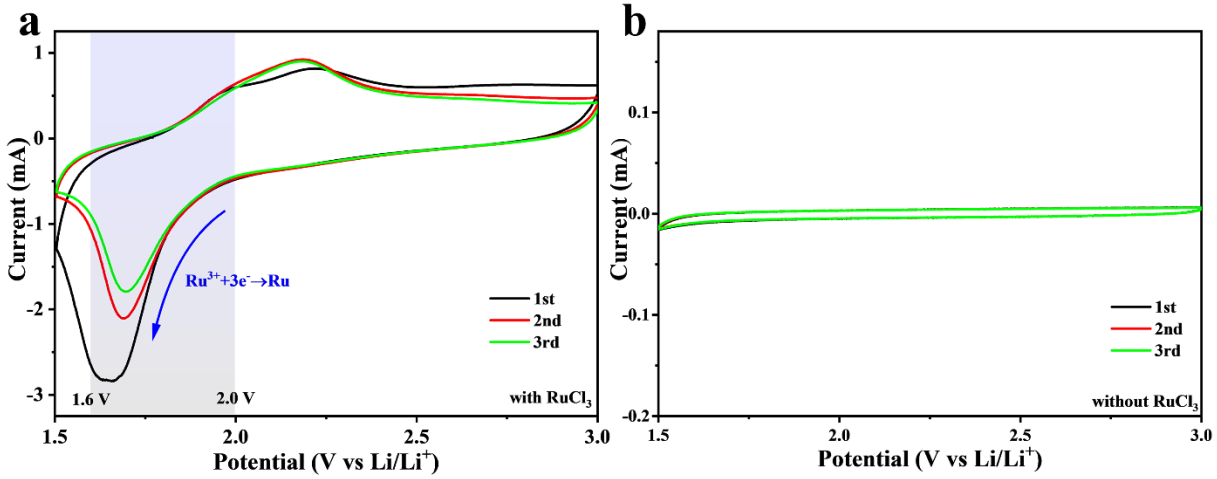

Fig. S3 (a-b) CV curves of Li||C cell within 1.5~3.0 V at a scan rate of 0.2 mV s^{-1} with $RuCl_3$ or without $RuCl_3$, respectively.

We think the reduction peak is attributed to the Ru(III) reduction with $RuCl_3$ during the discharging process (**Fig.** S3a). In **Fig.** S3b, there is no reduction peak during the cathodic scanning in the CV curve of Li||C cell without $RuCl_3$.

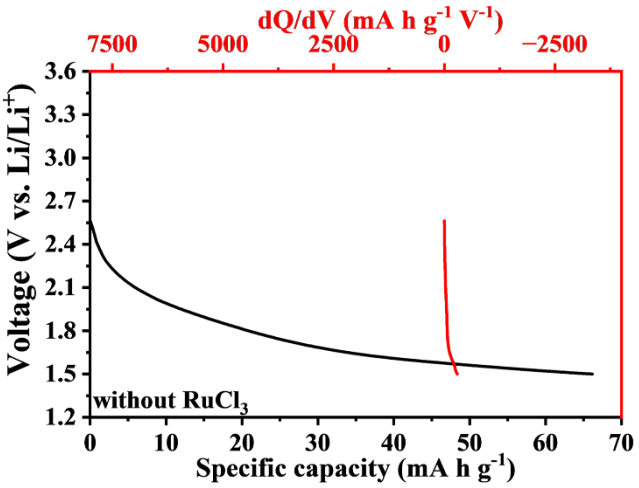

Fig. S4 Discharge and dQ/dV curves of the Li||C cell without $RuCl_3$.

There is no reduction peak at 1.8 V in the dQ/dV curve for the Li||C cell without $RuCl_3$, which further demonstrates the feasibility of Ru(III) reduction in cells (**Fig.** S4).

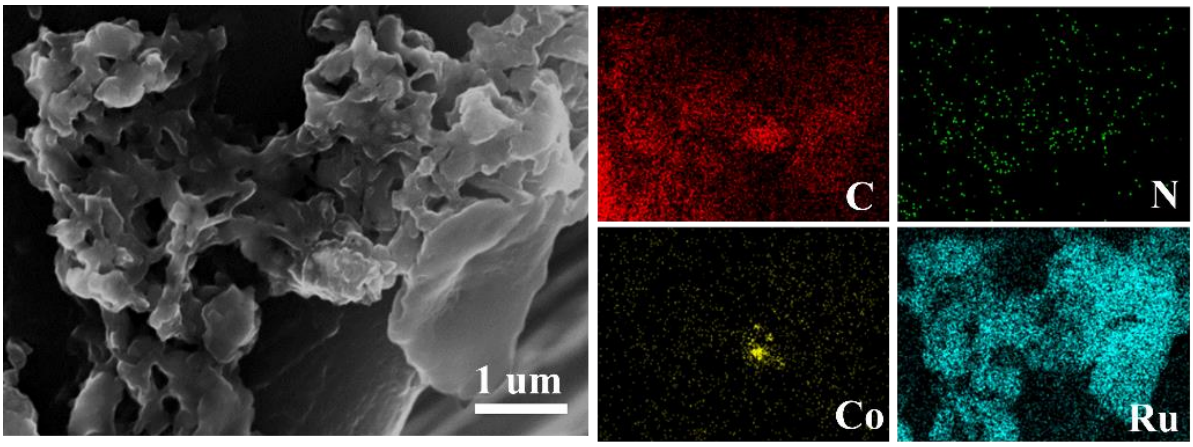

Fig. S5 FESEM image, C, N, Co, and Ru element mappings of ultrafine Ru-based cathode.

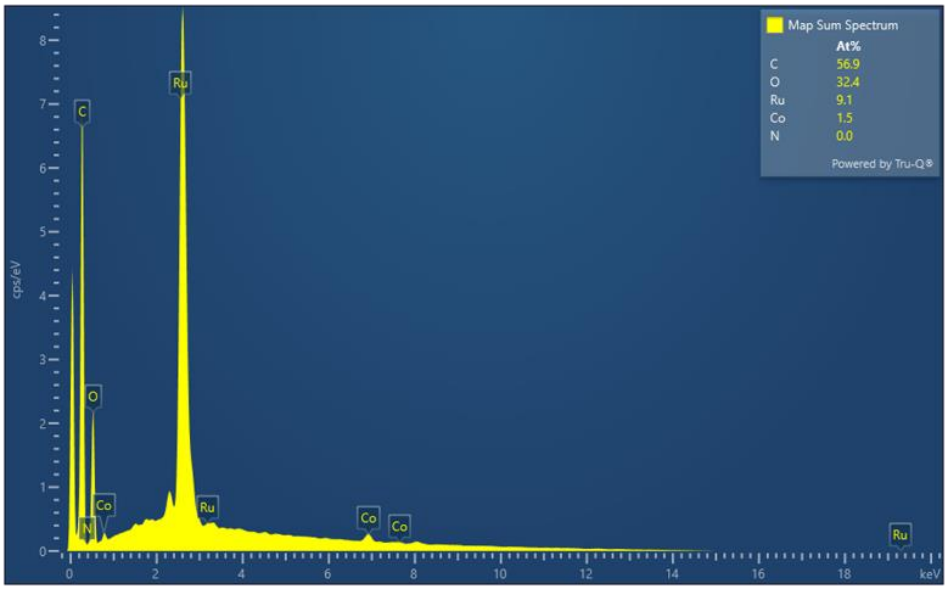

Fig. S6 The EDS analysis of ultrafine Ru-based catalyst.

In addition, the EDS result in **Fig.** S6 reveal that the Ru species and Co atoms are 9.1 and 1.5 at%, confirming the successful loading of Ru. The content of N cannot be detected by the EDS analysis due to the low content of N and high-content carbon from the background. Therefore, we provided XPS and element mappings to analyze the atomic percentage of N in an ultrafine Ru-based cathode. Doped N content is 2.32 at% on the surface of the ultrafine Ru-based cathode.

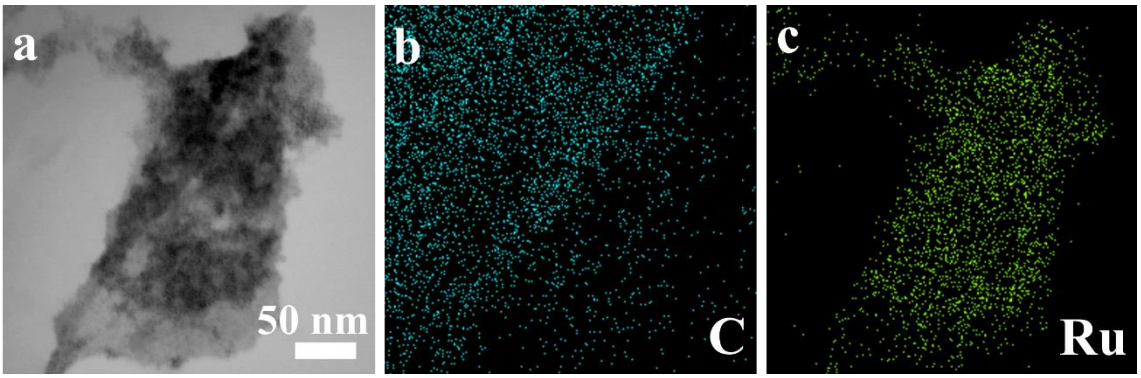

Fig. S7 STEM image, with C and Ru element mappings of Ru/CP cathode.

We added ultrafine Ru nanoparticles on carbon paper (Ru/CP) by in-situ reduction method in **Fig.** S7. The STEM and Ru mapping confirmed that the nanoparticles are nano-Ru. However, Ru nanoparticles agglomerated due to the small surface area of pure carbon paper.

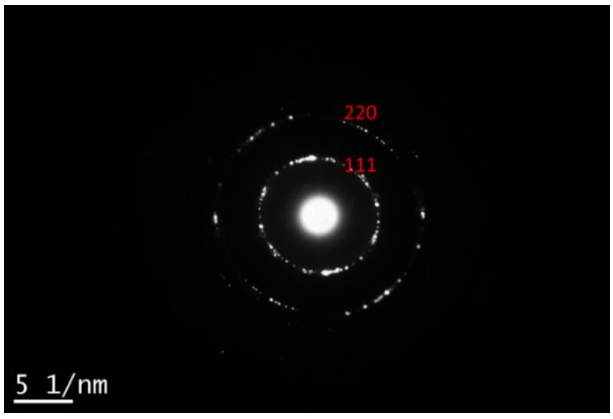

Fig. S8 The selected area electron diffraction pattern of ultrafine Ru-based catalyst.

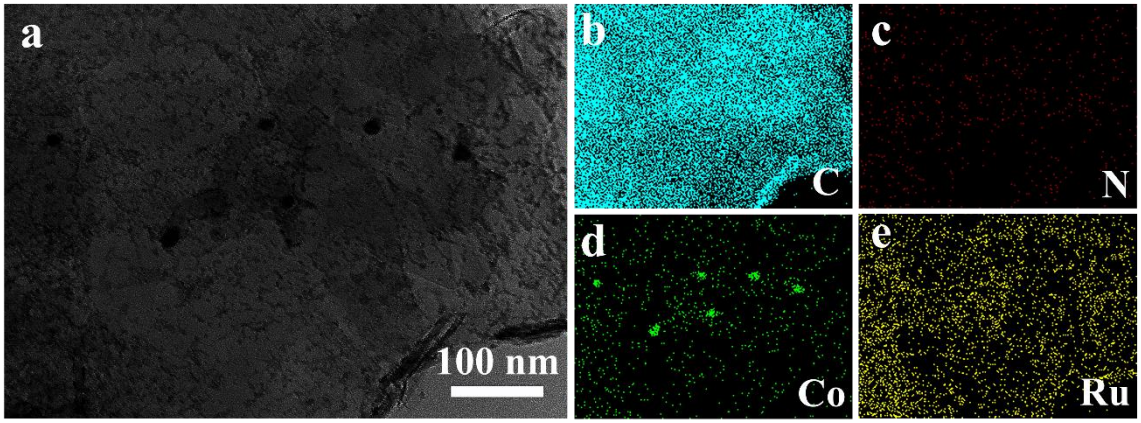

Fig. S9 STEM image; C, N, Co, and Ru element mappings of ultrafine Ru-based cathode.

The Co-NC material was obtained through high-temperature pyrolysis, in which the metal Co nanoparticles are formed and coated by multilayer graphitized carbon, rather than the aggregation of Co (**Fig.** S9).

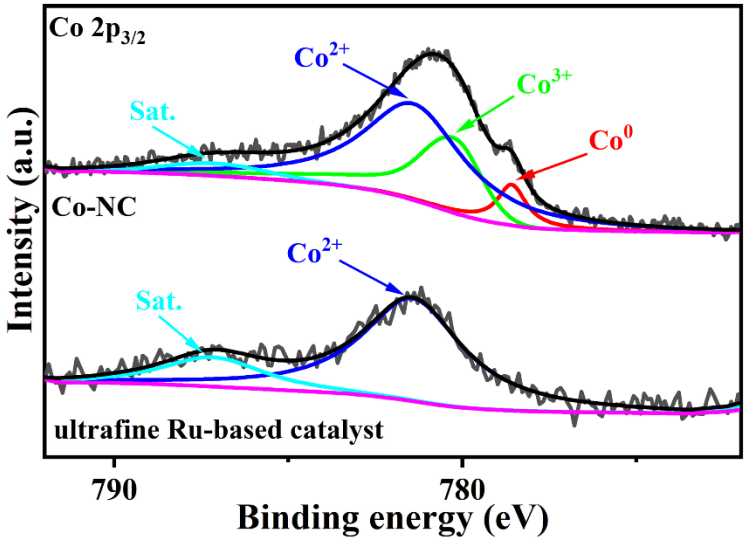

Fig. S10 High-resolution Co 2p XPS spectrum of Co-NC and ultrafine Ru-based catalyst.

We provided the fitted Co 2p XPS spectra of Co-NC and ultrafine Ru-based catalyst in **Fig.** S10. There is the existence of metallic Co^0 (778.6 eV), Co^{3+} (780.3 eV), Co^{2+} (781.4 eV), and satellite peaks in fitted Co 2p XPS spectrum. After loading Ru, the Co^0 element could not be fitted because Co was covered by nano-Ru and graphitized carbon and only Co^{2+} (781.4 eV) was fitted in the ultrafine Ru-based cathode, indicating that absorbed Co^{3+} on the surface is reduced to Co^{2+} after discharge.

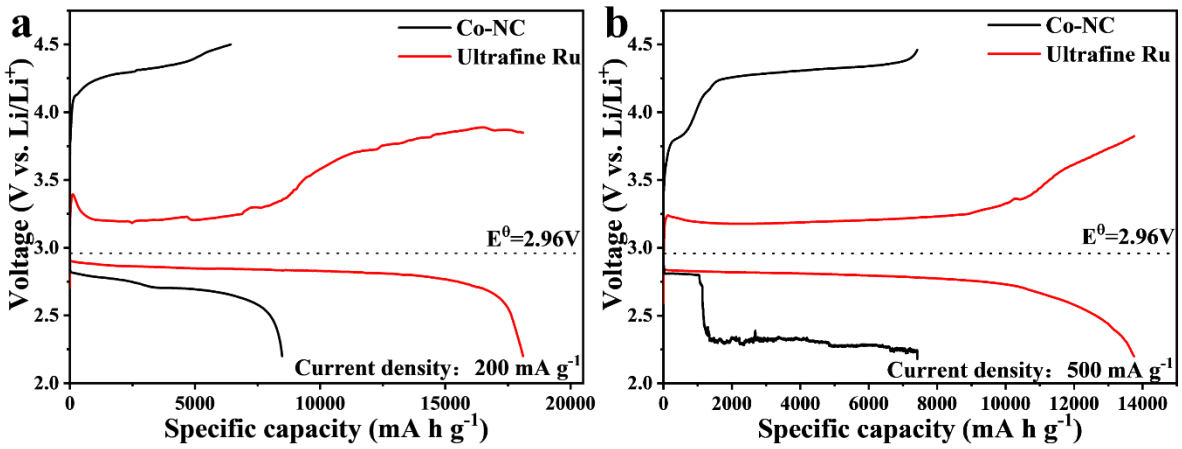

Fig. S11 (a-b) The initial full discharge/recharge curves of two cathodes at a current density of 200 and 500 mA g^{-1}, respectively.

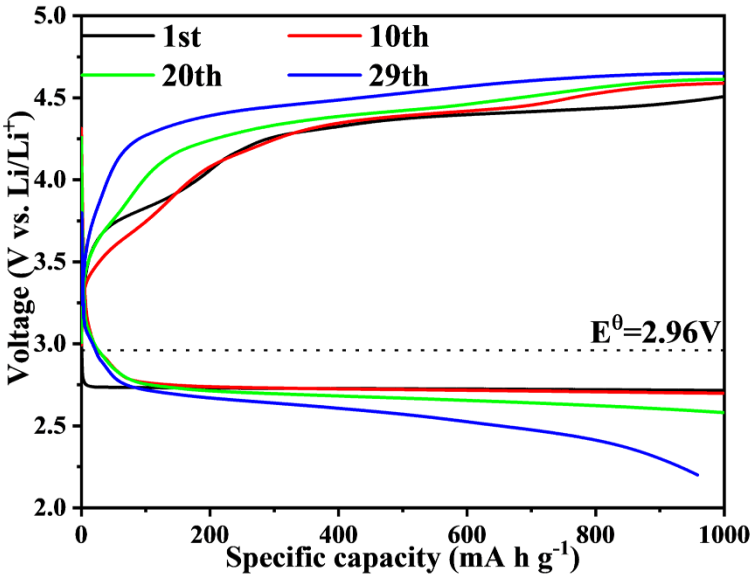

Fig. S12 The long cycling tests of LOBs with Co-NC cathode with a fixed specific capacity of 1000 mA h g^{-1} at 500 mA g^{-1}.

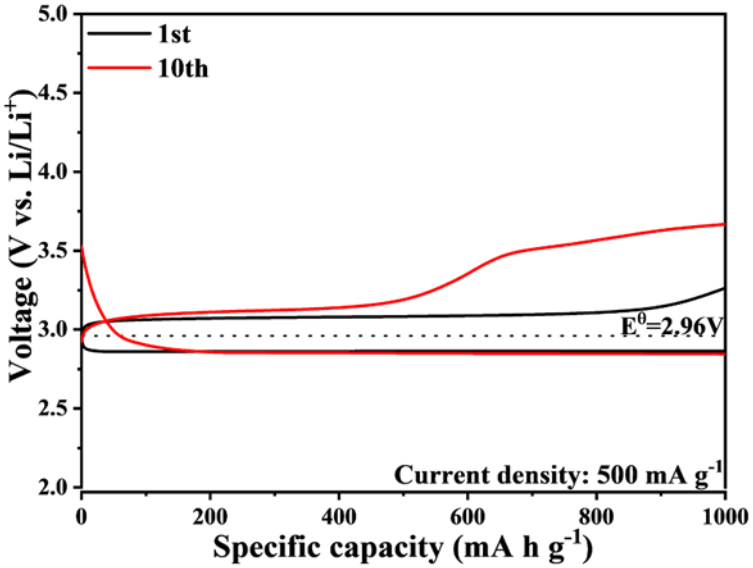

Fig. S13 The long cycling tests of LOBs with ultrafine Ru-based cathode with a fixed specific capacity of 1000 mA h g^{-1} at a current density of 500 mA g^{-1}.

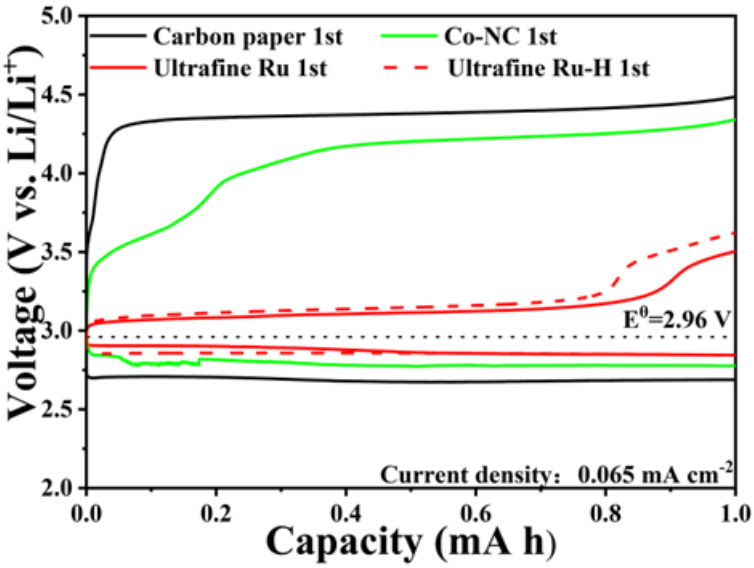

Fig. S14 The first discharge/charge curves of different cathodes with a fixed capacity of 1 mA h at a current density of 0.065 mA cm^{-2}.

Furthermore, we removed the Co on the surface of an ultrafine Ru-based electrocatalyst (Named ultrafine Ru-H cathode) by 1 M HCl solution to find out the influence of Co in LOBs. The discharge/charge performance of ultrafine Ru-H-based LOBs (**Fig.** S14) is also superior to the Co-NC electrode, indicating Co element on the surface has little contribution to reducing the overpotential of LOBs.

Carbon paper is used as the current collector with high quality of 8.36 mg cm^{-2}. To make the experiment more comparable, we further provided the catalysis performance based on the area of electrodes. **Fig.** S14 shows the discharge/charge curves of different cathodes.

The first discharge/charge curve is one of the most important criteria to measure the electrochemical performance of LOBs, so the discharge/charge curves of LOBs based on different cathodes were tested with a fixed capacity of 1 mA h at a current density of 0.065 mA cm^{-2}. It can be observed that the LOBs based on ultrafine Ru-based cathode (**Fig.** S14) show the highest discharge potential and lowest charge potential, which is much better than the carbon paper cathode and Co-NC cathode in the same condition. The impressive discharge/charge performance not only further confirms the excellent catalytic activity of ultrafine Ru-based cathode for LOBs, but also indicates its outstanding catalytic performance.

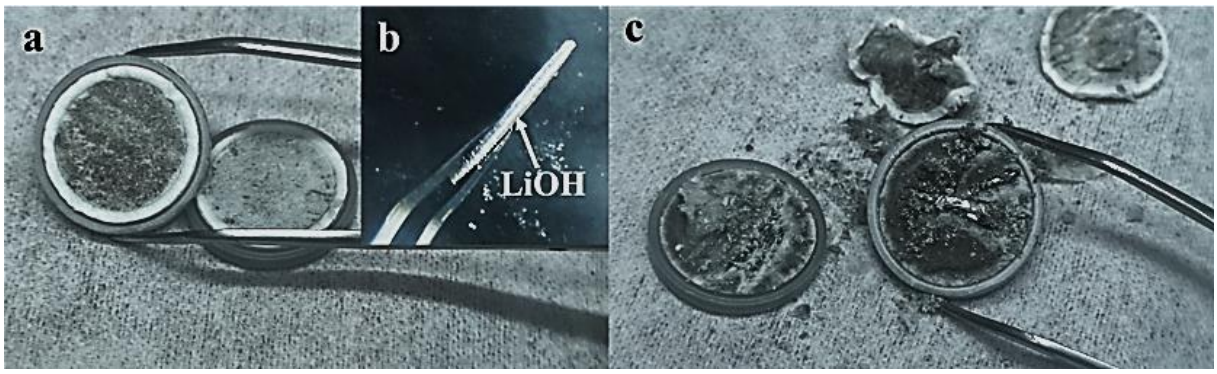

Fig. S15 (a-c) Optical images showing the change of a lithium slice and separator after long cycling tests of LOBs.

To find out the cause of death for LOBs, post-analysis was conducted to disassemble the cycled LOBs. In **Fig.** S15, the optical images show that a thicker LiOH was deposited on the surface of the lithium slice while the electrolyte is consumed after cycling for a long time, which will increase the internal resistance and reduce the performance of LOBs. We think the excellent performance of the electrocatalyst was attributed to uniformly dispersed fcc-Ru nanoparticles with high-active sites and excellent catalytic activity, which could improve the rate capability and the cycling performance of LOBs.

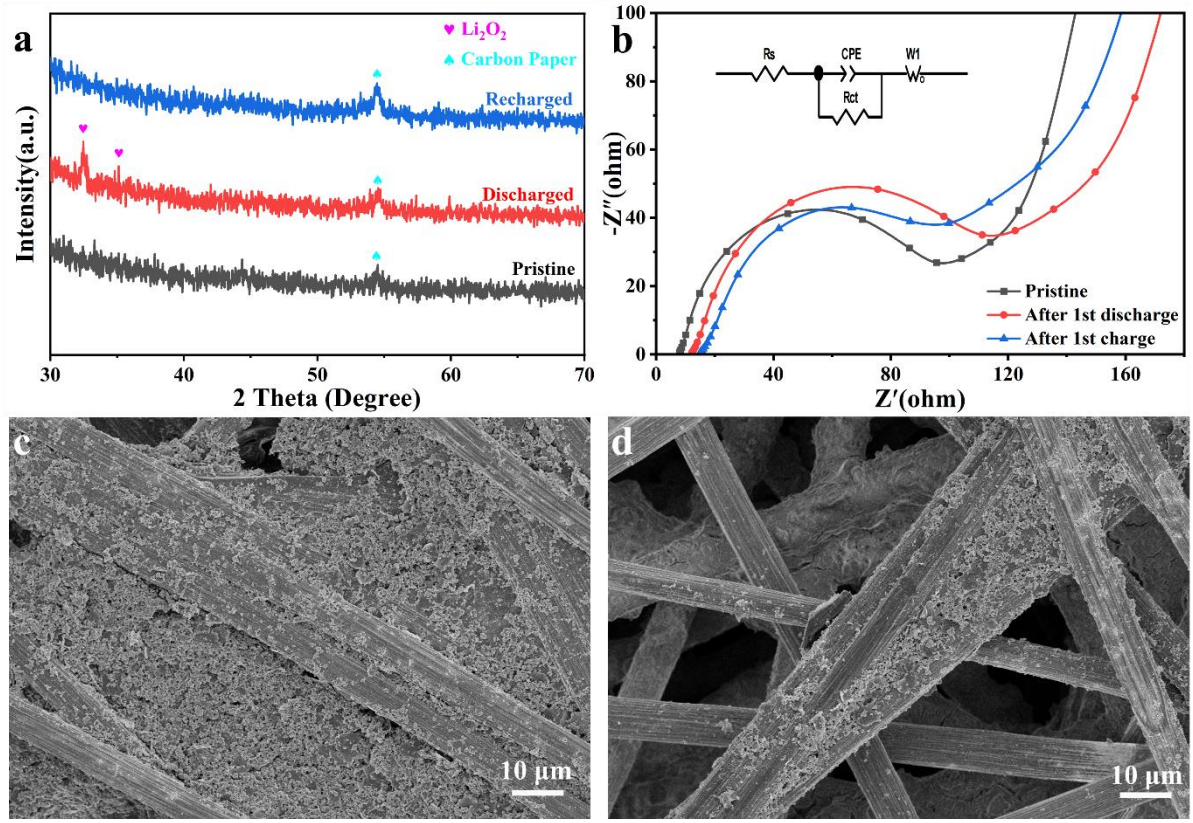

Fig. S16 (a) Ex-situ XRD patterns and (b) EIS curves of the pristine, fully discharged, and recharged ultrafine Ru-based cathodes, respectively. (c-d) Ex-situ FESEM images of the fully discharged and recharged ultrafine Ru-based cathodes, respectively.

Fig. S16b is the electrochemical impedance spectroscopy (EIS) spectra of Ru-based LOBs that were carried out to investigate the charge transfer kinetics. The pristine cathode shows a minimum charge transfer impedance of 84 Ω, indicating that there is good electronic/ionic conductivity at the electrode-electrolyte interface. After the first discharge, Li_2O_2 is formed on the ultrafine Ru-based cathode which leads to an increase of the charge transfer impedance. After the subsequent first charge, the charge transfer impedance is close to the value of the original cathode, indicating that the discharge product Li_2O_2 could be decomposed reversibly.[S3,4] **Fig.** S16c shows the ex-situ FESEM image of the ultrafine Ru-based cathode. Li_2O_2 is deposited on the cathode after being fully discharged to 2.20 V. Most of Li_2O_2 is decomposed reversibly after the full recharge (**Fig.** S16d), indicating that the prepared Ru-based catalyst has a good catalytic performance for the decomposition of Li_2O_2.

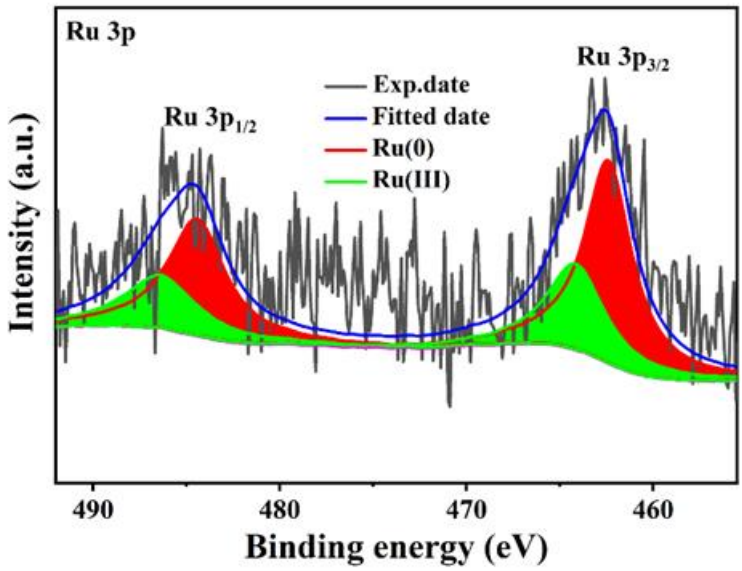

Fig. S17 High-resolution Ru 3p XPS spectrum of the ultrafine Ru-based cathode after three cycles.

To further examine the Ru chemical states on the cathode surface, we further supplemented the XPS data of the ultrafine Ru-based cathode after the galvanostatic discharge and recharge cycling test. Therefore, we provide XPS characterization of the catalyst materials after 3 cycles in **Fig.** S17. The ultrafine Ru-based cathode was still dominated with Ru (0) after three full cycles, indicating that Ru may be stable during the charging process in LOBs.

Table S1 Electrochemical performance comparison of ultrafine Ru-based LOBs with Ru-based LOBs.

Catalysts materials	Current density [mA g^{-1}]	ΔV (V)	Discharge capacity [mA h g^{-1}]	Cycle number [cycles] / cutoff capacities [mA h g^{-1}]	Ref.
Ru@MCN	1000	~0.8 V	~7000	100/2000	S2
Ru-chimera-CMT	1000	0.54 V	0.78 mA h	70/2000	S5
$Ru_{0.3}$ SAs-NC	0.02 mA cm^{-2}	0.55 V	13424	60/1000	S3
Ru/N-rGO	100	0.51 V	17074 at 500 mA g^{-1}	100/500	S4
FeN_x-HDC@Ru	200	0.93 V	3080	90/500	S6
Ru_{NC}/Co_{SA}-3DNG	200	0.84 V	~20000	300/1000	S7
Ru-V-CIS	400	~0.52 V at 200 mA g^{-1}	9170	200/1000	S8
NiRu-HTP	500	0.88 V	15080	200/1000	S9
Ru/Co@CoN_x–C	300	1.08 V	17050	205/1000	S10
Ru/Ti_4O_7	200	0.36 V	11000	/	S11
Fe_{SA}-RuO_2/HPCS	100	0.34 V	19891 at 200 mA g^{-1}	232/1000	S12
Ru SAs@MnO_2	0.05 mA cm^{-2}	0.69 V	7.74 mA h cm^{-1}	180/0.25 mA h cm^{-2}	S13
Co_2P/Ru/CNT	100	0.75 V	18048	185/1000	S14
Ultrafine nano-Ru	100 500	0.20 V 0.26 V	22754 13740	-- 185/1000	This work

References

S1. C. Yue, N. Zhang, Z. Zhu, P. Chen, F. Meng, X. Liu, X. Wei and J. Liu, *Small*, 2022, **18**, 2106532.

S2. L. Wei, Y. Ma, Y. Gu, X. Yuan, Y. He, X. Li, L. Zhao, Y. Peng and Z. Deng, *ACS Appl. Mater. Interfaces*, 2021, **13**, 28295-28303.

S3. X. Hu, G. Luo, Q. Zhao, D. Wu, T. Yang, J. Wen, R. Wang, C. Xu and N. Hu, *J. Am. Chem. Soc.*, 2020, **142**, 16776-16786.

S4. W. Dai, Y. Liu, M. Wang, M. Lin, X. Lian, Y. Luo, J. Yang and W. Chen, *ACS Appl. Mater. Interfaces*, 2021, **13**, 19915-19926.

S5. Z. Sun, C. Yang, F. Jiang and T. Zhang, *Adv. Funct. Mater.*, 2021, **31**, 2104011.

S6. L. Yao, J. Lin, S. Li, Y. Wu, H. Ding, H. Zheng, W. Xu, T. Xie, G. Yue and D. Peng, *J. Colloid Interface Sci.*, 2021, **596**, 1-11.

S7. M. Liu, J. Li, B. Chi, L. Zheng, Y. Zhang, Q. Zhang, T. Tang, L. Zheng and S. Liao, *J. Mater. Chem. A*, 2021, **9**, 10747-10757.

S8. R. Zheng, C. Shu, C. Liu, Y. Yan, M. He, M. Li, A. Hu and J. Long, *ACS Sustainable Chem. Eng.*, 2021, **9**, 7499-7507.

S9. Q. Lv, Z. Zhu, Y. Ni, B. Wen, Z. Jiang, H. Fang and F. Li, *J. Am. Chem. Soc.*, 2022, **144**, 23239–23246.

S10. Z. Tong, C. Lv, Y. Zhou, P. F. Zhang, C. C. Xiang, Z. G. Li, Z. Wang, Z. K. Liu, J. T. Li and S. G. Sun, *Small*, 2022, **18**, 2204836.

S11. X. Cao, C. Wei, X. Zheng, K. Zeng, X. Chen, M. H. Rummeli, P. Strasser and R. Yang, *Energy Storage Materials*, 2022, **50**, 355-364.

S12. Z. Lian, Y. Lu, S. Zhao, Z. Li and Q. Liu, *Adv. Sci.*, 2023, **10**, 2205975.

S13. B. Liu, X. Liu, C. Wei, Y. Zhou, Z. Zhu, X. Lei, Y. Fang, Y. Zhang, J. Liu, Y. Qian and G. Wang, *J. Mater. Chem. A*, 2023, **11**, 1188-1198.

S14. P. Wang, C. Li, S. Dong, X. Ge, P. Zhang, X. Miao, Z. Zhang, C. Wang and L. Yin, *Small*, 2019, **15**, 1900001.